Atomic-scale origin of dynamic viscoelastic response and creep in disordered solids

Rico Milkus[1] and Alessio Zaccone[1,2]

[1]*Statistical Physics Group, Department of Chemical Engineering and Biotechnology, University of Cambridge, New Museums Site, Cambridge CB2 3RA, United Kingdom*

[2]*Cavendish Laboratory, University of Cambridge, J. J. Thomson Avenue, Cambridge CB30HE, United Kingdom*

(Received 19 September 2016; published 1 February 2017)

Viscoelasticity has been described since the time of Maxwell as an interpolation of purely viscous and purely elastic response, but its microscopic atomic-level mechanism in solids has remained elusive. We studied three model disordered solids: a random lattice, the bond-depleted fcc lattice, and the fcc lattice with vacancies. Within the harmonic approximation for central-force lattices, we applied sum rules for viscoelastic response derived on the basis of nonaffine atomic motions. The latter motions are a direct result of local structural disorder, and in particular, of the lack of inversion symmetry in disordered lattices. By defining a suitable quantitative and general atomic-level measure of nonaffinity and inversion symmetry, we show that the viscoelastic responses of all three systems collapse onto a master curve upon normalizing by the overall strength of inversion-symmetry breaking in each system. Close to the isostatic point for central-force lattices, power-law creep $G(t) \sim t^{-1/2}$ emerges as a consequence of the interplay between soft vibrational modes and nonaffine dynamics, and various analytical scalings, supported by numerical calculations, are predicted by the theory.

DOI: 10.1103/PhysRevE.95.023001

I. INTRODUCTION

The viscoelasticity of solids has been the object of intense debate at least since the time of Maxwell. Continuum mechanics and relaxation models have flourished throughout the last century, with many extensions proposed to capture different behaviors observed in metallurgy [1,2]. For crystals with line defects, Andrade creep [whereby the relaxation shear modulus presents the power-law scaling $G(t) \sim t^{-1/3}$] has been convincingly explained by Nabarro, Mott, and others in terms of dislocation dynamics [3,4]. Internal friction, which represents the imaginary part of the viscoelastic response also known as the loss modulus G'', has been interpreted in earlier models, in terms of the diffusive motion of atoms associated with defect mobility.

In glasses the situation is more complicated, because dislocations are difficult to identify, and the origin of internal friction and complex relaxation behavior observed typically (power law or stretched exponential) has remained unexplained. A recent work [5] has applied elegant field-theoretic methods within the coherent-potential approximation, starting from the assumption of a spatially heterogeneous static shear modulus, to successfully recover the α-wing asymmetry in the resonance peak of G'' in oscillatory rheology observed in experiments. However, the theory is on the continuum level, and does not clarify which microscopic (atomic-level) features ultimately control the viscoelastic response.

Recent simulation work [6] motivated by this problem, in the context of metallic glasses, has shown that internal friction in glasses may have its origin in quasilocalized correlated motions that have an avalanchelike character. Furthermore, these excitations were found to be suppressed in regions of high icosahedral symmetry. Power-law creep $G \sim t^{-1/2}$ was recovered in previous work using mean field theory [7] and average stress fluctuations [8]. The same result was found in a related field of athermal jammed solids, where simulations and scaling arguments [9,10] based on Kelvin-Voigt viscoelasticity have been combined with the asymptotics of the vibrational density of states (DOS) near the jamming transition (at which a jammed solid loses rigidity) with average contact number $Z = 6$, although the strongly nonaffine motion of the particles, which is crucial for disordered and jammed solids [11,12], was not explicitly taken into account in the scaling analysis [9]. We improve on these methods by explicitly taking into account the exact microstructure of the system as well as the nonaffine motions of all particles, and we provide a direct link between the structure, the vibrational dynamics and the frequency- and time-dependent shear modulus.

II. MODEL SYSTEMS

Here, we reexamine this problem by considering three very different model systems of amorphous solids in three dimensions (3D), of which two-dimensional (2D) slices are given in Fig. 1. We will work with a specific model of disordered harmonic spring networks formed from the low-T equilibration of dense Lennard-Jones fluids. This is a good model for atomic disordered solids (defective crystals, metallic glasses) but different from other types of disordered networks where the preparation protocol may change the critical exponents and the critical coordination numbers for the onset of rigidity [13–16].

The first lattice is a random network of harmonic springs generated according to the protocol in Ref. [17]: A Lennard-Jones glass is formed and equilibrated in a metastable minimum, after which all nearest-neighbor interactions are replaced by harmonic springs, all with the same spring constant κ and with a relatively narrow distribution of spring length R_0. Upon randomly cutting the harmonic bonds in the sample, lattices with variable coordination number Z can be formed. In the present work this depletion process is performed in such a way that we get a very narrow distribution of coordination numbers to avoid effects stemming from fluctuating connectivity in the system.

The two fcc lattices [the bond-depleted, Fig. 1(b), and with vacancies, Fig. 1(c)] are instead generated starting

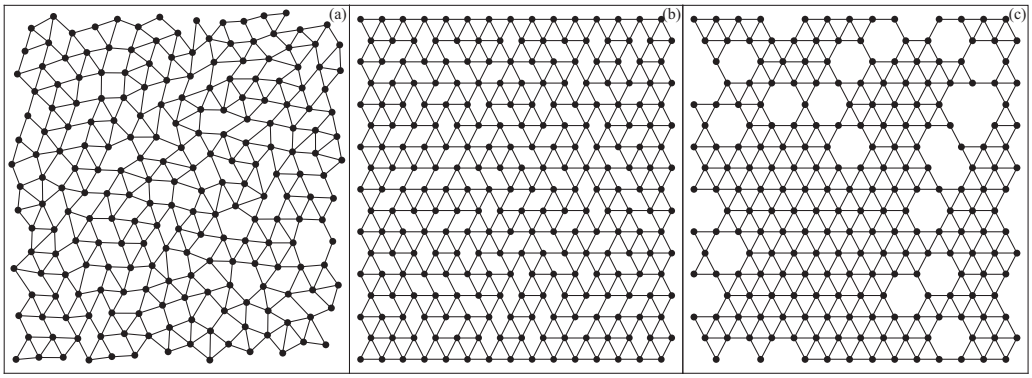

FIG. 1. Two-dimensional schematic of our 3D model systems. (a) The random network, (b) the fcc lattice with randomly cut bonds, and (c) the fcc lattice with randomly removed atoms.

from a perfect fcc lattice with $Z = 12$ and the same spring constant κ and lattice constant R_0 as the random lattice. The microstructure, and, in particular, the local symmetry, of the three lattices is, however, very different. For example, in Ref. [17] it was shown that the standard bond-orientational order parameter F_6, which measures the spread in the orientations of bonds on the lattice [18], is practically equal to 1 for the bond-depleted fcc (for any Z value), whereas it is much lower ($\simeq$0.3) for the random lattice.

For these models we develop an analytical theory of viscoelastic response based on the nonaffine deformation formalism, which is a fully microscopic approach. Our analysis shows that, surprisingly, the oscillatory moduli of these systems fall onto a master curve after normalizing by an order parameter which describes the average degree of local inversion symmetry on any atom. The same order parameter controls the nonaffine particle rearrangements that have a cooperative quasilocalized character, which explains the findings of simulations [6]. Further, the power-law creep $G \sim t^{-1/2}$ found near the isostatic transition of all the three lattices is shown to be the consequence of both the excess of soft modes in the DOS, and, crucially, also of the underlying nonaffine dynamics.

III. FORMALISM

The starting point of our analysis is the microscopic equation of motion for a particle in a disordered lattice, which was derived by Lemaitre and Maloney for the case of a phenomenological damping motion with constant damping coefficient ν, in Ref. [19], and was shown, also in Ref. [19], to reduce to a simple harmonic-oscillator type equation for the deviation variable $\underline{x}_i$, which measures the particle displacement from the original position:

$$m\ddot{\underline{x}}_i + \nu\dot{\underline{x}}_i + \underline{\underline{H}}_{ij}\underline{x}_j = \underline{\Xi}_{i,\kappa\chi}\eta_{\kappa\chi}. \tag{1}$$

We used the Hessian of the system $\underline{\underline{H}}_{ij} = -\partial^2\mathcal{U}/\partial\underline{r}_i\partial\underline{r}_j = -\partial\underline{f}_i/\partial\underline{r}_j$ and the nonaffine force $\underline{\Xi}_{i,\kappa\chi} = \partial\underline{f}_i/\partial\eta_{\kappa\chi}$. Here, $\eta_{\kappa\chi}$ denotes the Cauchy strain tensor for a generic deformation field. For a shear deformation, $\kappa\chi \equiv xy$. The nonaffine force $\underline{\Xi}_{i,\kappa\chi}$ represents the net force that acts on a particle that is en route towards its affine position. If the particle's original position in the undeformed lattice is $\underline{R}_0$, the affine position is defined as $\underline{r}_{i,A} = \underline{\underline{\eta}}\underline{R}_{i,0}$. In a perfectly centrosymmetric lattice, the particle en route towards this affine position receives forces from its nearest neighbors which cancel each other out by symmetry, leaving the particle at equilibrium in the affine position. In a disordered lattice, due to local breaking of inversion symmetry on the given particle, these forces do not cancel, and their vector sum is a net force that brings the particle to a final (nonaffine) position which differs from $\underline{r}_{i,A}$. For a generic harmonic lattice with no prestress, the nonaffine force vector is defined as $\underline{\Xi}_{i,\alpha\beta} = -R_0\kappa\sum_j \hat{n}^\alpha_{ij}\hat{n}^\beta_{ij}\underline{\hat{n}}_{ij}$, with R_0 and κ being the rest distance and force constant between the particles. The sum is performed over the nearest neighbors and includes the unit bond vector $\underline{\hat{n}}_{ij}$ pointing from atom i to j.

Normal-mode decomposition of the terms in Eq. (1) onto the eigenvectors $\underline{v}_p$ (where $p = 1 \ldots N$) of the Hessian, and taking the Fourier transform of the equation of motion as in Ref. [19], lead to the complex viscoelastic shear modulus for oscillatory shear deformation (with imposed frequency Ω):

$$G^*(\Omega) = G^A - 3\rho\int_0^{\omega_D}\frac{D(\omega)\Gamma(\omega)}{m\omega^2 - m\Omega^2 + i\nu\Omega}d\omega. \tag{2}$$

Here, we introduced the frequency correlator of the nonaffine forces, $\Gamma_{xyxy}(\omega) = \langle\hat{\Xi}_{p,xy}\hat{\Xi}_{p,xy}\rangle_{p\in\{\omega,\omega+\delta\omega\}}$, where $\hat{\Xi}_{p,xy} = \underline{\Xi}_{xy}\cdot\underline{v}_p$. Also, $\rho = N/V$ is the atomic density, or number of atoms (or nodes) on the lattice per unit volume. G^A is the affine shear modulus (also known as the Born-Huang modulus), which is independent of the applied frequency Ω, and coincides with the elastic response in the limit $\Omega \to \infty$. Here, ω denotes the eigenmode frequency of internal vibrations of the lattice, and ω_D denotes the Debye frequency, i.e., the highest frequency of the vibrational spectrum. The latter spectrum, i.e., the normalized distribution of vibrational eigenmodes is represented by the DOS, denoted here as $D(\omega)$. The mass of the particles m is set to 1 for the reminder of the paper, since it is of no concern in the present work.

The above sum rule allows the calculation of the complex shear modulus for any harmonic lattice for which both the DOS and the correlator function $\Gamma(\omega)$ can be easily evaluated numerically. For the DOS we follow the same procedure as in Ref. [17], whereas for $\Gamma(\omega)$ we follow the procedure of Ref. [19]. This is a straightforward exercise for the three model lattices shown in Fig. 1.

IV. RESULTS

We have calculated $G^*(\Omega)$ for the three lattices with two different average coordination numbers, $Z = 7.0$, where all lattices are mechanically well stable, $Z = 6$ (for the fcc with vacancies) and $Z = 6.1$ (for the two bond-depleted systems), i.e., at or close to the point of marginal stability. First, we calculated the vibrational density of states $D(\omega)$ and the correlator function $\Gamma(\omega)$, which are shown in Fig. 2. Since these quantities appear as the $D(\omega)\Gamma(\omega)$ product in Eq. (2), it is convenient to study this product as a single function of ω.

Remarkably, we notice from Fig. 2 that, although $D(\omega)$ and $\Gamma(\omega)$ behave differently for each of the three systems and have a rather complicated form, their product, when normalized by the quantity $\langle|\underline{\Xi}|^2\rangle/\rho$, shows a strikingly *universal* behavior over the full frequency range, and can be fitted by a simple cubic function of ω, of the form

$$\frac{D(\omega)\Gamma(\omega)}{\langle|\underline{\Xi}|^2\rangle/\rho} \sim \omega^2(\omega_D - \omega). \tag{3}$$

Here, the quantity $\langle|\underline{\Xi}|^2\rangle$ is evaluated by taking the square of the absolute value of each vector $|\underline{\Xi}_i|$, constructed for each atom i, and averaging over all atoms in the system. This same quantity has been used to form a suitably normalized order parameter in Ref. [17].

Since $D(\omega)$ approaches a low-ω plateau in the limit of marginal stability ($Z \to 6$), as is known from many studies in the past [20,21]), the low-frequency behavior of $D(\omega)\Gamma(\omega)$ is dominated by the correlator function $\Gamma(\omega) \sim \omega^2$, a result that was derived in Ref. [22]. It is interesting to note Dirac-delta spikes in $\Gamma(\omega)$, which happen at frequencies that correspond to strongly localized modes: At $Z = 6$ a spike is visible near the top of the spectrum, where modes tend to be Anderson localized. At $Z = 7$, instead, a spike is visible at a frequency close to the Ioffe-Regel crossover [23] (and to the boson peak frequency) where modes are also strongly localized [17].

Let us now consider the viscoelastic response of the three model systems. We use the convention of splitting the complex shear modulus into its real and imaginary part

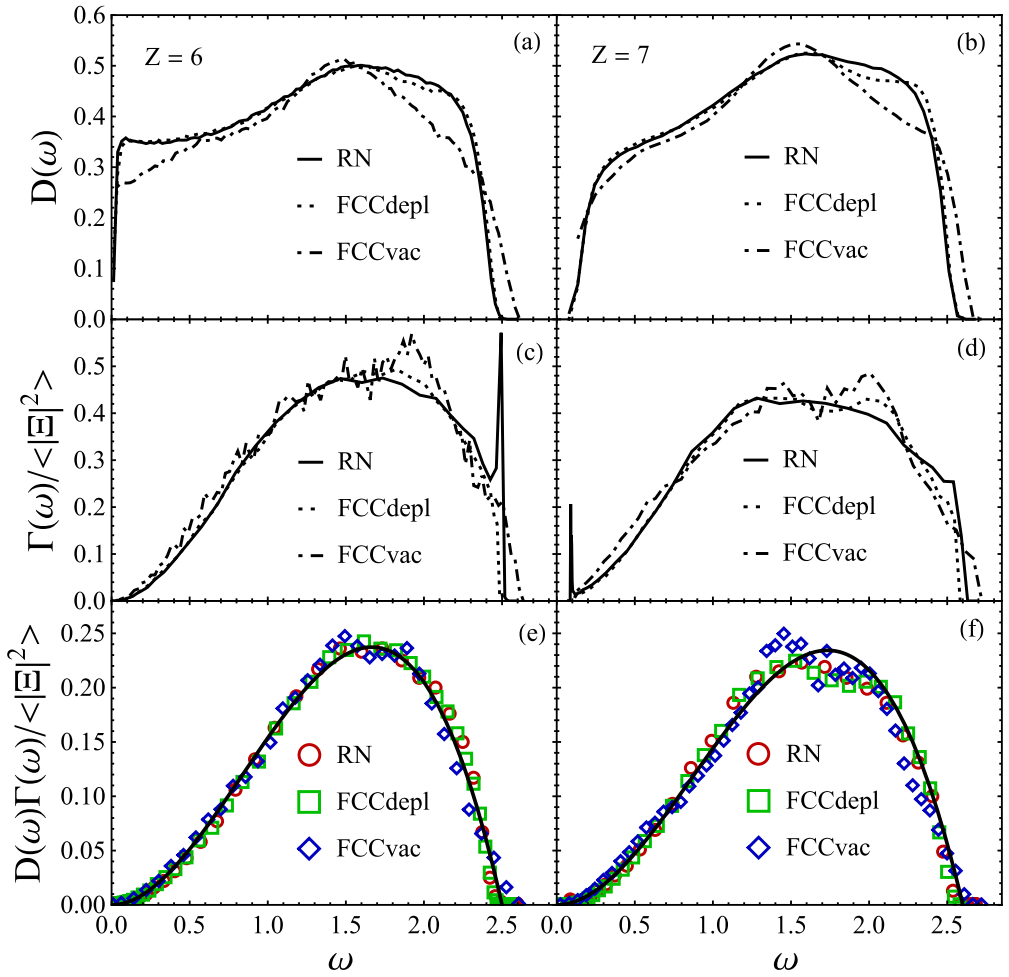

FIG. 2. (a), (b) Density of states $D(\omega)$ and (c), (d) correlator function $\Gamma(\omega)$ for the three different model systems and two different coordination numbers ($Z = 6.1$ and $Z = 7$, respectively). They are normalized by $\langle|\underline{\Xi}|^2\rangle/\rho$, proportional to the average absolute square of the nonaffine force field to obtain a master curve. (e) and (f) show the product $D(\omega)\Gamma(\omega)$ which appears in the formula for $G^*(\Omega)$. Remarkably, the product of the two functions can be conveniently fitted by a simple cubic function $\omega^2(\omega_D - \omega)$, represented as a solid line.

$G(\Omega) = G'(\Omega) + iG''(\Omega)$. Both moduli can be calculated according to

$$G'(\Omega) = G^A - 3\rho \int_0^{\omega_D} \frac{D(\omega)\Gamma(\omega)(\omega^2 - \Omega^2)}{(\omega^2 - \Omega^2)^2 + \nu^2\Omega^2}, \quad (4)$$

$$G''(\Omega) = 3\rho \int_0^{\omega_D} \frac{D(\omega)\Gamma(\omega)\nu\Omega}{(\omega^2 - \Omega^2)^2 + \nu^2\Omega^2}, \quad (5)$$

and are plotted in Fig. 3. In the numerical calculation we implemented the convenient cubic form of the product $D(\omega)\Gamma(\omega)$ that was shown above to be an excellent fitting to the numerical evaluation of these functions. Various scalings have been reported in the plots, which can be extracted from the asymptotic analysis of Eqs. (4) and (5), most notable of which are the low-frequency scalings of $G''(\Omega)$, which agree very well with the Effective Medium Theory (EMT) results from Ref. [7] ($G'' \sim \Omega^{1/2}$ for $Z \approx 6$ and $G'' \sim \Omega$ for $Z = 7$). Deviations from their numerical results ($G'' \sim \Omega^{0.41}$) might be caused by finite temperature effects in their simulations (whereas our calculation is carried out at $T = 0$). In our work we have used different values of the damping coefficient ν to study its influence on the results. We found that it has no influence on the qualitative behavior of G' and G'', besides when it approaches very small values, where we get divergent results. Aside from that, ν only shifts the values to smaller Ω and expands the range of the $\sim\Omega^{-1}$ scaling in G''. We therefore chose a quite large value $\nu = 10'000$ to demonstrate this behavior clearly and to focus on the physically important case of overdamped dynamics typical of amorphous solids (metallic glasses, organic glasses, foams, etc.).

Next, we consider the time-dependent shear modulus $G(t)$, which can be calculated by taking the inverse Fourier transform of $G^*(\Omega)$,

$$G(t) = G - \frac{3}{2\pi}\rho \int_{-\infty}^{\infty}\int_0^{\infty} \frac{D(\omega)\Gamma(\omega)\exp(i\Omega t)}{\omega^2 - \Omega^2 + i\nu\Omega} d\omega d\Omega$$
$$= G - 3\rho t e^{-\frac{\nu}{2}t} \int_0^{\infty} D(\omega)\Gamma(\omega)\mathrm{sinc}\left(\frac{1}{2}\sqrt{4\omega^2 - \nu^2}t\right)d\omega. \quad (6)$$

Here, G is the infinite-time static shear modulus (which has a strong nonaffine character), and $\mathrm{sinc}(x) = \sin(x)/x$ denotes the cardinal sine function. Numerical evaluations of Eq. (6) for the three lattices at the two representative values of Z are reported in Fig. 4. Again, we took advantage of the simple cubic fitting Eq. (3) for the product $D(\omega)\Gamma(\omega)$, which allows one to avoid the problem of a numerical gap between zero frequency and the first eigenfrequency (this gap is not negligible for systems with $N < 10^5$ and our simulated lattices have $N = 5 \times 10^4$). For small times we observe a plateau that corresponds to the high-frequency affine response, after which a power-law decay is observed with an exponent comprised in the range between $-1/2$ and $-3/4$. This power law can be understood mechanistically as follows.

We focus on the limit of overdamped systems, which is both important and turns out to be amenable to analytic simplifications. For large ν and large times we can simplify the expression in Eq. (6). First, we take $\sqrt{\nu^2 - 4\omega^2} \approx \nu - 2\frac{\omega^2}{\nu}$, where we use $\omega \ll \nu$. We insert this into Eq. (6) and use the

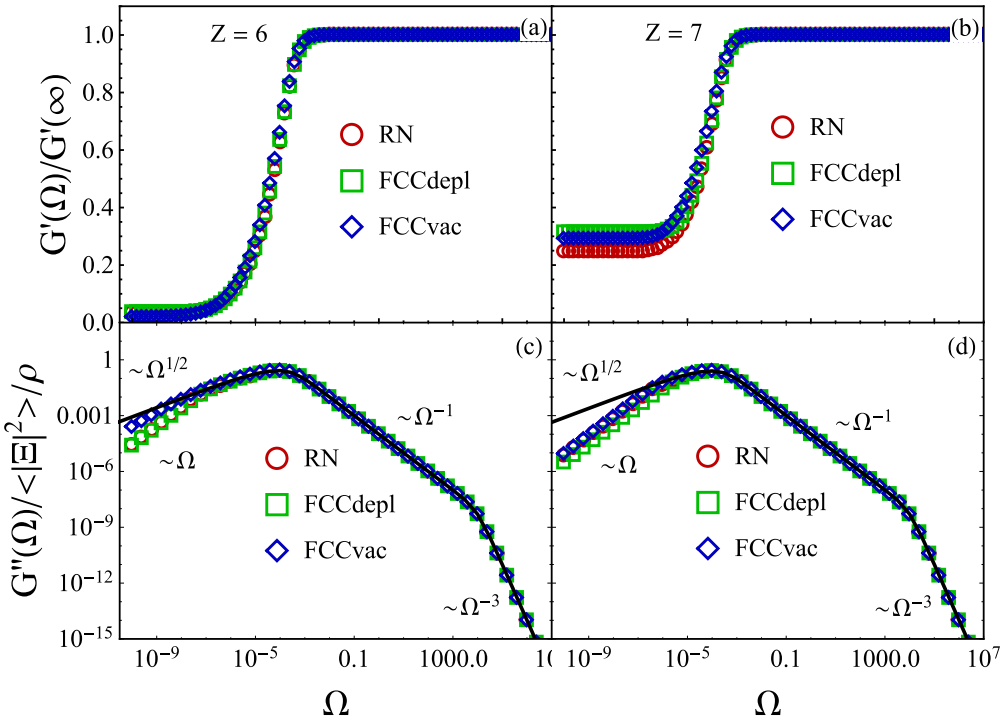

FIG. 3. (a), (b) G' and (c), (d) G'' of our three model systems for $Z = 6$ (left) and $Z = 7$ (right), respectively. In (c) and (d) in order to collapse the loss modulus of the three systems onto a single master curve, we have normalized by the factor $\langle|\Xi|^2\rangle/\rho$.

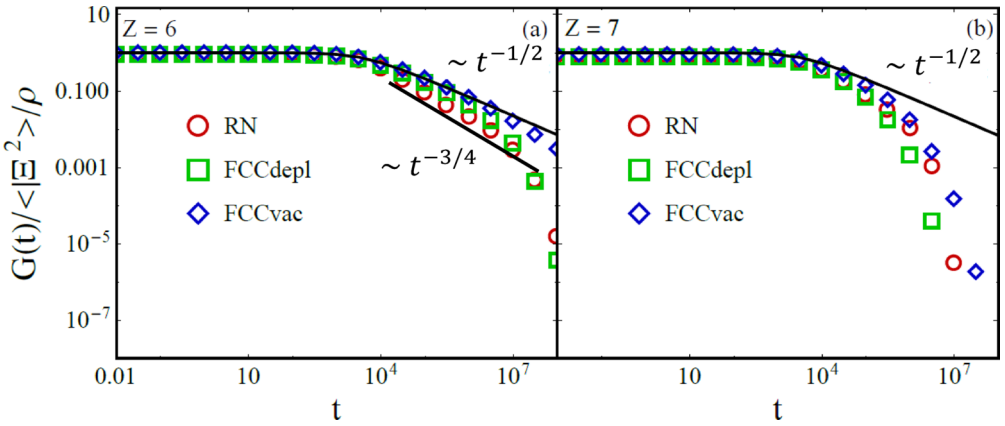

FIG. 4. $G(t)$ of our three model systems for $Z = 6$ (left) and $Z = 7$ (right). We have indicated the different scaling ranges. One can see that the power-law scaling, which is present on three to four orders of magnitude in time for $Z = 6$, breaks down for $Z = 7$. This is due to the Debye $\sim \omega^2$ regime in the DOS being broader for $Z = 7$ (see text).

definition of $\sinh(x)$ to get

$$G(t) \approx 6\rho e^{-\frac{\nu}{2}t} \int_0^\infty \frac{D(\omega)\Gamma(\omega)\sinh\left(\frac{\nu}{2}t - \frac{\omega^2}{\nu}t\right)}{\omega^2\left(\nu - 2\frac{\omega^2}{\nu}\right)} d\omega$$
$$= 3\rho \int_0^\infty \frac{D(\omega)\Gamma(\omega)\left(e^{-\frac{\omega^2}{\nu}t} - e^{-\nu t + \frac{\omega^2}{\nu}t}\right)}{\omega^2\left(\nu - 2\frac{\omega^2}{\nu}\right)} d\omega$$
$$\approx 3\rho \frac{1}{\nu} \int_0^\infty \frac{D(\omega)\Gamma(\omega)}{\omega^2} e^{-\frac{\omega^2}{\nu}t} d\omega. \quad (7)$$

In the last step we have used $\nu \gg 2\omega^2/\nu$ and $\nu t - \omega^2 t/\nu \gg 1$. This corresponds to a system of Maxwell elements with relaxation times $\tau = \nu/\omega^2$. We now recall the standard relationship between the DOS and the eigenvalue spectrum $\rho(\lambda)$ of the Hessian matrix, $D(\omega)d\omega = \rho(\lambda)d\lambda$, with $\omega^2 = \lambda$. At the isostatic point of disordered solids, $Z = 6$, the DOS develops a plateau of soft modes, which is visible in our Fig. 2(a). This limit corresponds to the scaling $\rho(\lambda) \sim \lambda^{-1/2}$ in the eigenvalue distribution, which arises from the dominance of random-matrix behavior in the spectrum, and this scaling can be derived, e.g., from the famous Marcenko-Pastur distribution of random-matrix theory, as discussed recently in Ref. [24]. In our DOS, a scaling $\rho(\lambda) \sim a + \lambda^{-1/2}$, where a is a constant, is more appropriate since we are in fact slightly above $Z = 6$, and this will explain the power-law exponents in $G(t)$ being larger than $1/2$ in our calculations. However, we will stick to the simple $\rho(\lambda) \sim \lambda^{-1/2}$ for the asymptotic analysis. Recall now that $\Gamma(\omega) \sim \omega^2$, from the analytical theory of nonaffine deformations [22], which implies $\tilde{\Gamma}(\lambda) \sim \lambda$. Inserting these results in the last line of Eq. (7), we obtain the following Laplace transform which can be easily evaluated

$$G(t) \sim \int_0^\infty \frac{\rho(\lambda)\tilde{\Gamma}(\lambda)}{\lambda} e^{-\lambda t} d\lambda$$
$$\sim \int_0^\infty \frac{\lambda^{-1/2}\lambda}{\lambda} e^{-\lambda t} d\lambda \sim t^{-1/2}. \quad (8)$$

This scaling for the power-law creep modulus was shown in simulations of creep in athermal jammed systems in the important work of Ref. [9], using a system of Kelvin-Voigt elements (whereas we use a standard-linear solid or Zener material). The theoretical argument that was proposed to explain the scaling $t^{-1/2}$ was not fully microscopic, because the correlator between eigenmodes and shear field was taken to be independent of the eigenfrequency, hence constant on average for a given frequency interval. This is not a physically justified approximation, because the correlator $\Gamma(\omega)$ in our data (and also in Ref. [19]) displays a strong (and nonrandom) dependence on the eigenfrequency, as one can see in Figs. 3(c) and 3(d). Our model improves substantially on this aspect, by including the eigenfrequency dependence of the nonaffine correlator into the theoretical analysis of the scaling. In this way, our framework provides a direct link between the microscopic nonaffine dynamics and the viscoelastic moduli.

V. CONCLUSION

Using the nonaffine response formalism, we studied three model harmonic lattices with disorder, which have very different microstructures (as reflected in, e.g., different values of bond-orientational order parameter as shown in previous work [17]). Yet, the three different lattices have qualitatively the same (universal) viscoelastic response, i.e., G' and G'' collapse onto master curves as a function of frequency, once the moduli are normalized by a factor $\langle|\underline{\Xi}|^2\rangle/\rho$, where ρ is the atomic density. Here, $\langle|\underline{\Xi}|^2\rangle$ is crucially related to the symmetry that controls this universality, i.e., the local degree of inversion symmetry. This is evident from the definition of the nonaffine force vector for harmonic lattices, $\underline{\Xi}_{i,xy} = -R_0\kappa \sum_j \hat{n}^x_{ij}\hat{n}^y_{ij}\underline{\hat{n}}_{ij}$. The norm of this vector is clearly identically zero for all atoms in a perfectly centrosymmetric lattice with no defects, whereas its value is larger for lattices where the inversion symmetry is lowered. Hence, the parameter $\langle|\underline{\Xi}|^2\rangle$ crucially is proportional to the overall (spatially averaged) degree to which local inversion symmetry is broken in a disordered lattice.

These results thus identify the atomic-scale origin of internal friction and viscoelastic response in amorphous solids (e.g., glasses) with the local inversion-symmetry breaking, which

is the same effect that causes a softer elastic response [17] and is associated with quasilocalized avalanchelike nonaffine motions [25]. Our framework provides a clear theoretical explanation of recent simulation results [6] where internal friction was shown to correlate with cooperative nonaffine motions and regions of lower local centrosymmetry. This framework will play an important role in the rational design of new materials with tailored viscoelastic response and energy absorption properties in many materials science and engineering applications.

[1] C. M. Zener, *Elasticity and Anelasticity of Metals* (University of Chicago Press, Chicago, 1948).

[2] R. de Batist, *Internal Friction of Structural Defects in Crystalline Solids* (North-Holland, Amsterdam, 1973).

[3] N. F. Mott, A theory of work-hardening of metals. 2. Flow without slip-lines, recovery and creep, Philos. Mag. **44**, 742 (1953).

[4] F. R. N. Nabarro, Thermal activation and Andrade creep, Philos. Mag. **75**, 227 (2010).

[5] W. Schirmacher, G. Ruocco, and V. Mazzone, Heterogeneous Viscoelasticity: A Combined Theory of Dynamic and Elastic Heterogeneity, Phys. Rev. Lett. **115**, 015901 (2015).

[6] H.-B. Yu and K. Samwer, Atomic mechanism of internal friction in a model metallic glass, Phys. Rev. B **90**, 144201 (2014).

[7] M. G. Yucht, M. Sheinman, and C. P. Broedersz, Dynamical behavior of disordered spring networks, Soft Matter **9**, 7000 (2013).

[8] A. J. Liu, S. Ramaswamy, T. G. Mason, H. Gang, and D. A. Weitz, Anomalous Viscous Loss in Emulsions, Phys. Rev. Lett. **76**, 3017 (1996).

[9] B. P. Tighe, Relaxations and Rheology near Jamming, Phys. Rev. Lett. **107**, 158303 (2011).

[10] B. P. Tighe, Dynamic Critical Response in Damped Random Spring Networks, Phys. Rev. Lett. **109**, 168303 (2012).

[11] F. Leonforte, R. Boissiere, A. Tanguy, J. P. Wittmer, and J.-L. Barrat, Continuum limit of amorphous elastic bodies. III. Three-dimensional systems, Phys. Rev. B **72**, 224206 (2005).

[12] C. E. Maloney and A. Lemaitre, Amorphous systems in athermal, quasistatic shear, Phys. Rev. E **74**, 016118 (2006).

[13] W. G. Ellenbroek, Z. Zeravcic, W. van Saarloos, and M. van Hecke, Non-affine response: Jammed packings vs. spring networks, Europhys. Lett. **87**, 34004 (2009).

[14] C. P. Lubensky, X. M. Mao, T. C. Lubensky, and F. C. MacKintosh, Criticality and isostaticity in fibre networks, Nat. Phys. **7**, 983 (2011).

[15] W. G. Ellenbroek, V. F. Hagh, A. Kumar, M. F. Thorpe, and M. van Hecke, Rigidity Loss in Disordered Systems: Three Scenarios, Phys. Rev. Lett. **114**, 135501 (2015).

[16] C. Buss, C. Heussinger, and O. Hallatschek, Thermalized connectivity networks of jammed packings, Soft Matter **12**, 7682 (2016).

[17] R. Milkus and A. Zaccone, Local inversion-symmetry breaking controls the boson peak in glasses and crystals, Phys. Rev. B **93**, 094204 (2016).

[18] P. J. Steinhardt, D. R. Nelson, and M. Ronchetti, Bond-orientational order in liquids and glasses, Phys. Rev. B **28**, 784 (1983).

[19] A. Lemaitre and C. Maloney, Sum rules for the quasistatic and viscoelastic response of disordered solids at zero temperature, J. Stat. Phys. **123**, 415 (2006).

[20] C. S. O'Hern, L. E. Silbert, A. J. Liu, and S. R. Nagel, Jamming at zero temperature and zero applied stress: The epitome of disorder, Phys. Rev. E **68**, 011306 (2003).

[21] L. E. Silbert, A. J. Liu, and S. R. Nagel, Vibrations and Diverging Length Scales Near the Unjamming Transition, Phys. Rev. Lett. **95**, 098301 (2005).

[22] A. Zaccone and E. Scossa-Romano, Approximate analytical description of the nonaffine response of amorphous solids, Phys. Rev. B **83**, 184205 (2011).

[23] H. Shintani and H. Tanaka, Universal link between the boson peak and transverse phonons in glass, Nat. Mater. **7**, 870 (2008).

[24] S. Franz, G. Parisi, P. Urbani, and F. Zamponi, Universal spectrum of normal modes in low-temperature glasses, Proc. Natl. Acad. Sci. USA **112**, 14539 (2015).

[25] A. Widmer-Cooper, H. Perry, P. Harrowell, and D. R. Reichman, Irreversible reorganization in a supercooled liquid originates from localized soft modes, Nat. Phys. **4**, 711 (2008).